Incomplete proteasomal degradation of green fluorescent proteins in the context of tandem fluorescent protein timers

Anton Khmelinskii, Matthias Meurer, Chi-Ting Ho, Birgit Besenbeck, Bernd Bukau, Axel Mogk, Michael Knop*

Zentrum für Molekulare Biologie der Universität Heidelberg (ZMBH) and Deutsches Krebsforschungszentrum (DKFZ), DKFZ-ZMBH Alliance, Im Neuenheimer Feld 282, 69120 Heidelberg, Germany
*Correspondence to M.K. (m.knop@zmbh.uni-heidelberg.de)

Running Head

Proteasomal processing of tFTs

Abbreviations

tFT – tandem fluorescent protein timer
FP – fluorescent protein
greenFP – green fluorescent protein
redFP – red fluorescent protein

Abstract

Tandem fluorescent protein timers (tFTs) report on protein age through time-dependent change in color, which can be exploited to study protein turnover and trafficking. Each tFT, composed of two fluorescent proteins (FPs) that differ in maturation kinetics, is suited to follow protein dynamics within a specific time range determined by the maturation rates of both FPs. So far tFTs were constructed by combining different slower-maturing red fluorescent proteins (redFPs) with the same faster-maturing superfolder green fluorescent protein (sfGFP). Towards a comprehensive characterization of tFTs, we compare here tFTs composed of different faster-maturing greenFPs, while keeping the slower-maturing redFP constant (mCherry). Our results indicate that the greenFP maturation kinetics influences the time range of a tFT. Moreover, we observe that commonly used greenFPs can partially withstand proteasomal degradation due to the stability of the FP fold, which results in accumulation of tFT fragments in the cell. Depending on the order of FPs in the timer, incomplete proteasomal degradation either shifts the time range of the tFT towards slower time scales or precludes its use for measurements of protein turnover. We identify greenFPs that are efficiently degraded by the proteasome and provide simple guidelines for design of new tFTs.

Introduction

Fluorescent proteins (FPs) become fluorescent only upon correct folding of the polypeptide and formation of the fluorophore through a series of chemical reactions within the β-barrel fold. This maturation process takes place on time scales from minutes to hours, depending on the FP and the environment (Tsien, 1998; Shaner *et al.*, 2005). The time delay between protein synthesis and completion of the maturation process is exploited in tandem fluorescent protein timers (tFTs) to measure the dynamics of various cellular processes (Khmelinskii *et al.*, 2012). A tFT is a fusion of two FPs that differ in maturation kinetics and spectral properties (i.e. color), e.g. a slower-maturing red fluorescent protein (redFP) and a faster-maturing green fluorescent protein (greenFP) (Figure 1A). The greenFP is typically selected to be as fast-maturing as possible and thus reports on protein localization and abundance. Because of the difference in maturation kinetics between the greenFP and redFP moieties, the color of a tFT (defined as the redFP/greenFP ratio of fluorescence intensities) changes over time (Figure 1A). When a tFT is fused to a protein of interest, its color provides a measure of protein age that can be used to follow protein degradation, trafficking and segregation during cell division (Khmelinskii *et al.*, 2012).

The range of protein ages that can be analyzed with a tFT, i.e. its time range, is strongly influenced by the maturation kinetics of the slower-maturing FP in the pair (Khmelinskii *et al.*, 2012). Therefore, in the tFTs described thus far (Khmelinskii *et al.*, 2012; Dona *et al.*, 2013; Khmelinskii and Knop, 2014), different slower-maturing redFPs (mCherry, TagRFP, DsRed1) were combined with the same faster-maturing superfolder green fluorescent protein (sfGFP) (Pédelacq *et al.*, 2006). Several properties make sfGFP a greenFP of choice for construction of tFTs: it is bright, it folds independently of the protein it is fused to, it is one of the

faster-maturing greenFPs, with a maturation half-time of ~6 min in yeast (Pédelacq *et al.*, 2006; Khmelinskii *et al.*, 2012), and an additional V206R mutation ensures it is monomeric (Zacharias *et al.*, 2002). Nevertheless, there is a wide range of greenFPs with other desirable properties such as high molecular brightness or high photostability (Dean and Palmer, 2014). However, their *in vivo* maturation rates, which determine their suitability for construction of new tFTs (Figure 1B), are not well characterized.

Here we sought to compare the performance of different greenFPs within tFTs. We constructed a series of mCherry-greenFP timers and examined their suitability for comparative measurements of protein age and protein degradation kinetics in yeast. We identified the stability of the greenFP fold as a new parameter that affects tFT behavior and directs the design and use of tFT as reporters of protein degradation.

Results

We constructed new putative tFTs by fusing the slower-maturing red fluorescent protein mCherry (Shaner *et al.*, 2004) to different greenFPs: the commonly used monomeric yeast codon-optimized enhanced GFP (myeGFP) (GFPmut 3a from (Cormack *et al.*, 1996) with the V206R dimerization-preventing mutation (Zacharias *et al.*, 2002)), the fast-maturing GFPm (Yoo *et al.*, 2007; Iizuka *et al.*, 2011), and two greenFPs with superior brightness – Clover (Lam *et al.*, 2012) and mNeonGreen (Shaner *et al.*, 2013) (Figure S1, A and B). myeGFP, GFPm, Clover and mNeonGreen have red-shifted excitation peaks compared to sfGFP. Using such greenFPs is likely to improve signal-to-noise ratio in fluorescence imaging as autofluorescence of yeast cells and growth media is substantially reduced with excitation wavelengths longer than 488 nm (Figure S1C).

To test whether these mCherry-greenFP fusions function as timers and to compare their ability to report on protein age, we analyzed cells expressing the proton pump Pma1 tagged with each putative tFT. Pma1 is an exceptionally stable protein of the plasma membrane (Thayer *et al.*, 2014). During yeast bud formation, pre-existing Pma1 molecules at the plasma membrane are retained in the mother cell, while the bud (future daughter cell) receives newly produced Pma1 (Takizawa *et al.*, 2000; Malínská *et al.*, 2003). Consequently, cells expressing Pma1 tagged with the mCherry-sfGFP timer exhibit lower mCherry/greenFP intensity ratios (R) at the plasma membrane in the bud (R_b) than in the mother cell (R_m) (Figure 1C) (Khmelinskii *et al.*, 2012). We observed the same trend for all Pma1 fusions (Figure 1D), indicating that all tested mCherry-greenFP variants function as timers. The R_b/R_m ratio can be used for a qualitative comparison of greenFP maturation kinetics with an approximate model of tFT maturation (Figure 1B) (Khmelinskii *et al.*, 2012). The R_b/R_m ratio was lowest for mCherry-sfGFP and mCherry-mNeonGreen timers (Figure 1D), indicating that sfGFP and mNeonGreen have the fastest maturation among all tested greenFPs. Consistent with slower maturation of Clover (Figure S1A), the R_b/R_m ratio was highest for the strain expressing Pma1-mCherry-Clover (Figure 1D).

We proceeded to examine the performance of all tFTs in comparative analysis of protein degradation kinetics. In steady state, the mCherry/greenFP intensity ratio is determined by the degradation kinetics of the tFT fusion, such that strains expressing rapidly degraded fusions are expected to exhibit lower mCherry/greenFP intensity ratios (Figure 2A) (Khmelinskii *et al.*, 2012). We generated two constructs for expression of N-terminal ubiquitin (Ubi) fusions with each tFT (Ubi-X-mCherry-greenFP): one with a methionine residue (M) and another with an arginine residue (R) at position X (Figure 2B). Co-translational cleavage of the ubiquitin moiety exposes a new N-terminus starting with residue X, which determines the stability of the fusion according to the N-end rule. Fusions with N-terminal arginine, but not with N-terminal methionine, are recognized by the E3 ubiquitin ligase Ubr1 and targeted for proteasomal degradation (Bachmair *et al.*, 1986; Varshavsky, 2011) (Figure S2, A and B). Accordingly, for each tFT, the mCherry/greenFP intensity ratio was lower for the strain expressing Ubi-R-mCherry-greenFP (Figure 2C), indicating that all tested tFTs report on protein degradation kinetics.

The difference between the median mCherry/greenFP intensity ratios of strains expressing Ubi-M-mCherry-greenFP and Ubi-R-mCherry-greenFP fusions varied from ~ 5 fold for the mCherry-sfGFP timer to 1.4 – 2.1 fold for the other tFTs. Comparison of these differences to an approximate model of tFT turnover (Figure 2A, Supplemental Theory) revealed several inconsistencies between theory and experiment. For instance, the relative mCherry/greenFP intensity ratio of Ubi-R-mCherry-sfGFP was considerably lower than expected (Figure 2, A and C). Moreover, tFTs with Clover and mNeonGreen exhibited similar relative mCherry/greenFP intensity ratios for Ubi-R-mCherry-greenFP (Figure 2C), despite the difference in maturation kinetics (Figure S1A) and distinct performance as reporters of protein age (Figure 1D). These observations suggest that a parameter other than greenFP maturation kinetics influences tFT behavior in the

protein degradation assay. Immunoblotting of whole cell extracts with antibodies against GFP (or against an haemagglutinin (HA) epitope fused to the C-terminus of mNeonGreen) revealed a product of mCherry autohydrolysis during cell extract preparation (Baird *et al.*, 2000) and unexpected tFT fragments around 33 kDa (~6 kDa larger than free greenFP) in all strains expressing Ubi-X-mCherry-greenFP fusions (Figure 2D). These fragments were most prominently seen for the tFT with sfGFP, especially for the Ubi-R-mCherry-sfGFP fusion. We sought to determine the origin of these protein fragments (hereafter referred to as processed tFT fragments) and to examine whether their presence can account for the unexpected behavior of different tFTs described above.

Two mechanisms could generate processed tFT fragments: proteolytic cleavage of the tFT by an endopeptidase (model 1) and incomplete degradation of the tFT by the proteasome (model 2) (Figure 3A). In model 1, the fraction of processed tFT in steady state ($\bar{G}$) is expected to be independent of the degradation kinetics of the tFT fusion. In contrast, $\bar{G}$ is expected to be proportional to the degradation kinetics of the tFT fusion in model 2 (further details in Supplemental Theory). Immunoblotting analysis of strains expressing a series of Ubi-X-mCherry-sfGFP fusions with different stabilities showed that the fraction of processed tFT increases as a function of protein degradation kinetics, in agreement with model 2 (Figure 3B). Moreover, accumulation of processed tFT fragments depended on proteasomal activity (Figure S2C). These observations were not specific to the Ubi-X-mCherry-greenFP fusions. Processed tFT fragments could also be detected in strains expressing misfolded cytoplasmic proteins tagged with mCherry-sfGFP and the fraction of processed tFT decreased upon deletion of E3 ubiquitin ligases involved in degradation of these misfolded proteins (Figure S2, D and E). Finally, similar ~33 kDa fragments have been observed when GFP fusions are degraded by proteasomes with impaired processivity, e.g. in mutants of the proteasome-associated E3 ubiquitin ligase Hul5 (or its mammalian ortholog UBE3C) (Zhang and Coffino, 2004; Aviram and Kornitzer, 2010; Martínez-Noël *et al.*, 2012; Chu *et al.*, 2013). We conclude that accumulation of processed tFT fragments is caused by incomplete proteasomal degradation of tFT fusions.

What features of the mCherry-sfGFP timer are responsible for its incomplete degradation? We considered two possibilities: the linker connecting mCherry to sfGFP and the robust fold of sfGFP. The linker between mCherry and greenFP in the tFTs is composed of a leucine (L) and an aspartate (D) residues followed by five glycine-alanine (GA) repeats ($LD(GA)_5$). GA rich sequences can prevent complete protein degradation by impairing the ability of the proteasome to unfold its substrate (Hoyt *et al.*, 2006; Daskalogianni *et al.*, 2008). To determine the role of the linker in the accumulation of processed tFT fragments, we tested shorter LDGAG or LDGS linker sequences between mCherry and sfGFP. Although shorter linkers changed the relative amounts of different processed tFT fragments, they did not reduce the total amount of processed fragments (Figure 4A) nor did they alter the ability of the mCherry-sfGFP timer to report on protein degradation kinetics (Figure 4B). In contrast, exchanging sfGFP for other greenFPs, while keeping the $LD(GA)_5$ linker between mCherry and greenFP constant, reduced the amount of processed tFT fragments (Figure 2D). This suggests that the greenFP moiety, not the linker, is responsible for incomplete degradation of tFT fusions.

To test the possibility that incomplete degradation is caused by the robust fold of sfGFP, we attempted to destabilize the sfGFP fold by reverting five mutations (S30R, Y39N, N105T, Y145F and I171V) responsible for the superfolder nature of sfGFP (Pédelacq *et al.*, 2006) ($sfGFP^{5M}$) or by reverting the F64L mutation known to improve GFP folding at 37°C (Tsien, 1998) ($sfGFP^{L64F}$). However, tFTs with these sfGFP mutants behaved similarly to the mCherry-sfGFP timer (Figure 4, C and D). Nevertheless, in a reverse experiment, introducing the F64L mutation into Clover increased the accumulation of processed tFT fragments in the strain expressing Ubi-R-mCherry-$Clover^{F64L}$ (Figure 4C). This accumulation correlated with a reduced mCherry/greenFP intensity ratio of Ubi-R-mCherry-$Clover^{F64L}$ relative to the Ubi-M-mCherry-$Clover^{F64L}$ fusion, bringing it close to Ubi-R-mCherry-sfGFP (Figure 4D). These observations support the idea that the stability of the greenFP fold is responsible incomplete degradation of tFT fusions.

Next we sought to destabilize the sfGFP fold through circular permutations. Circular permutation can drastically impair folding of classical GFP (Baird *et al.*, 1999; Topell *et al.*, 1999). Although sfGFP is largely tolerant of circular permutations (Pédelacq *et al.*, 2006), some circularly permutated sfGFP variants can be efficiently unfolded and more rapidly degraded by the AAA+ ClpXP protease *in vitro* (Nager *et al.*, 2011). We constructed a series of tFTs with different circular permutations (cp) of sfGFP and examined their behavior in the degradation assay with N-terminal ubiquitin fusions (Figure 4E). Accumulation of processed tFT fragments was reduced to below the detection limit with all circular permutations except cp3 (Figure 4F). This is consistent with higher mobility of the β_7-β_{11} sheets in the β-barrel fold and the tendency of GFP to start unfolding from β_7-β_{11} (Huang *et al.*, 2007; Zimmer *et al.*, 2014). As seen in the case of Clover (Figure 4D),

reduced accumulation of processed tFT fragments correlated with a reduced relative difference in mCherry/sfGFP ratios between the stable and unstable Ubi-X-mCherry-greenFP fusions (Figure 4G). Taken together, these experiments indicate that the stability of the greenFP fold is responsible for proteasome-dependent processing of tFTs and concomitant accumulation of tFT fragments.

Two permutations, cp7 and cp9, reduced the molecular brightness of sfGFP (Figure 4H). Another two, cp12 and cp13, appeared to affect protein folding and expression levels (Figure 4H, data not shown), and the maturation kinetics of sfGFP, as suggested by the lack of difference in mCherry/sfGFP ratios between the two Ubi-X-mCherry-greenFP fusions (Figure 4G). However, the cp8 permutation did not impair protein expression and had only a minor effect on the molecular brightness of sfGFP (Figure 4H). Moreover, sfGFP(cp8) exhibited the fastest maturation kinetics among all tested circular permutation, as evidenced by the performance of the mCherry-sfGFP(cp8) timer in the analysis of Pma1 protein age (Figure 1D). Therefore, sfGFP(cp8) represents an alternative to sfGFP without potential artifacts caused by incomplete proteasomal degradation.

We sought to determine how incomplete proteasomal degradation affects the properties of tFTs and their use in studies of protein dynamics. We incorporated proteasome-dependent processing into a model of tFT maturation and turnover for two tFTs, mCherry-sfGFP and sfGFP-mCherry. Proteasomal degradation typically requires an unstructured region in the substrate to initiate degradation (Prakash *et al.*, 2004). We assumed that no such initiation region is present in the mCherry-sfGFP and sfGFP-mCherry timers. It is implicit in the model that degradation is initiated within the tagged protein of interest and proceeds in a processive manner until the sfGFP fold is reached, at which point the remaining polypeptide can be either released from the proteasome with a defined probability or completely degraded. Incomplete degradation of proteins tagged at the C-terminus with mCherry-sfGFP or sfGFP-mCherry produces respectively free sfGFP or free sfGFP-mCherry in the model (further details in Supplemental Theory). Our experiments indicate that the mCherry-sfGFP timer functions as a degradation reporter with C-terminally tagged proteins (Figure 2) (Khmelinskii *et al.*, 2012). Theoretical analysis suggests that the time range of this timer is shifted toward more stable proteins when incomplete tFT degradation is considered, such that the difference in mCherry/sfGFP intensity ratios between Ubi-M-mCherry-sfGFP and Ubi-R-mCherry-sfGFP fusions is expected to increase with increasing probability of incomplete tFT degradation (Figure 5A). The experimentally observed behavior of Clover and sfGFP-based tFTs with different levels of incomplete tFT degradation is consistent with this prediction (Figure 4, D and G).

In contrast to the mCherry-sfGFP timer, incomplete degradation of the sfGFP-mCherry timer as a C-terminal tag is predicted to abolish the monotonic relationship between mCherry/sfGFP intensity ratio and protein half-life (Figure 5B). We tested this prediction in the degradation assay with N-terminal ubiquitin fusions. To ensure initiation of degradation N-terminally to sfGFP, we separated the N-terminal degradation signal (N-degron) from the sfGFP-mCherry timer with a spacer protein Don1 and an HA tag (Ubi-X-spacer-sfGFP-mCherry). Immunoblotting of whole cell extracts confirmed the accumulation of processed tFT fragments with the expected size, ~6 kDa larger than free sfGFP-mCherry, in these strains (Figure S3A). In contrast to strains expressing Ubi-X-mCherry-sfGFP fusions, the mCherry/sfGFP intensity ratio was largely independent of the degradation rate for Ubi-X-spacer-sfGFP-mCherry fusions (Figures 5C and S3B). This result is consistent with the model predictions and suggests that the probability of incomplete sfGFP degradation is substantial (~0.5 or higher) (Figure 5B). Moreover, it shows that the sfGFP-mCherry timer should not be used as a degradation reporter with C-terminally tagged proteins. However, it is important to stress that the sfGFP-mCherry fusion is a timer, i.e. it changes color with time, and thus should report on the age of C-terminally tagged proteins in the absence of protein degradation. Indeed cells expressing Pma1-sfGFP-mCherry exhibited lower mCherry/sfGFP intensity ratios at the plasma membrane in the bud than in the mother cell, similarly to Pma1-mCherry-sfGFP (Figure 1D). Moreover, the sfGFP-mCherry timer, but not the mCherry-sfGFP timer, faithfully reported on the degradation kinetics of N-terminally tagged proteins (Figures 5D and S3C). Together, these results indicate that different tFT variants should be used for N- and C-terminal protein tagging, such that the sfGFP moiety is placed distally to the region in the protein of interest where proteasomal degradation is initiated.

Discussion

We report here on the use of different greenFPs for analysis of protein dynamics with tFTs. All tested greenFPs can be combined with mCherry to obtain tFTs that report on protein age and degradation kinetics, indicating that greenFPs mature faster than mCherry. Our analysis shows that the greenFP maturation kinetics influences the time range of mCherry-greenFP timers (Figure 1). In addition, we observe that

greenFPs, and sfGFP in particular, can withstand proteasomal degradation in yeast (Figure 2), consistent with previous reports of incomplete proteasomal degradation of GFP (Zhang and Coffino, 2004; Aviram and Kornitzer, 2010; Martínez-Noël *et al.*, 2012; Chu *et al.*, 2013). Because of mCherry autohydrolysis during preparation of whole cell extracts (Baird *et al.*, 2000), we were not able to determine the efficiency of mCherry degradation by the proteasome. However, theoretical considerations suggest that incomplete proteasomal degradation of mCherry is likely to be negligible in yeast. If a substantial fraction of mCherry would withstand proteasomal degradation, no monotonic relationship between protein degradation kinetics and mCherry/sfGFP intensity ratio would be obtained with a C-terminal mCherry-sfGFP timer (Figure 5, B and C). The efficiency of FP degradation by the proteasome could differ in other organisms and cell types, as proteasome processivity varies between species (Kraut *et al.*, 2012).

Two features are necessary for a protein to become a proteasome substrate: a degradation signal (degron) and a degradation initiation site (Schrader *et al.*, 2009). These features are provided by the model substrates used to investigate tFT behavior in the degradation assay (Figure 2). Therefore, proteasomal degradation of a tFT starts from the site where it is linked to the model substrate and proceeds by unfolding and channeling of the polypeptide into the catalytic core of the 19S particle of the proteasome. Protein sequences that cannot be efficiently channeled into the catalytic core can be release from the proteasome. Several factors can contribute to this release: the protein sequence adjacent to the released domain, the stability of the fold of the released domain, and an intrinsic probability of the proteasome to release substrates that is independent of the power stroke underlying substrate unfolding (Kraut *et al.*, 2012; Fishbain *et al.*, 2015). Our analysis indicates that incomplete degradation of sfGFP fusions depends on the stability of the sfGFP fold (Figure 4), although the molecular details, i.e. the determinants in sfGFP, are unclear.

The outcome of proteasomal processing of tFT fusions depends on the order of FPs in the timer relative to the region in the protein from which proteasomal degradation begins. If mCherry is placed proximal to the degradation initiation site (e.g. in mCherry-sfGFP timer as a C-terminal tag), proteasomal processing produces tFT fragments of ~33 kDa (Figure 2). These contain the greenFP moiety and a short ~6 kDa tail that presumably corresponds to the length of the unfolded polypeptide channeled into the proteasome catalytic core before release of the fragments. In this situation, the timer functions as a reporter of protein age and degradation kinetics (Figure 5A). However, the increased cytoplasmic greenFP fluorescence resulting from incompete tFT degradation should be taken into account when measuring protein age at subcellular level. We note that the ~33 kDa tFT fragments are distinct from the ~26 kDa fragments observed upon incomplete lysosomal/vacuolar degradation of GFP fusions, which have been exploited to follow the cytoplasm to vacuole targeting (Cvt) pathway and autophagy (Shintani and Klionsky, 2004; Klionsky *et al.*, 2008). If in turn greenFP is located proximal to the degradation initiation site, proteasomal processing results in the release of ~60 kDa tFT fragments containing both FPs and a short ~6 kDa tail (Figure S3A). In this case the timer can be still used to measure local protein age but it no longer reports on protein degradation kinetics (Figure 5B). From these observations we can derive a short list of recommendations for design and use of tFTs as reporters of protein age and degradation:

(i) For tFTs based on mCherry and greenFPs, the FPs in the timer should be arranged such that the degradation-resistant greenFP ends up distal to the degradation initiation site in the tagged protein of interest. Thus, the mCherry-sfGFP timer should be used for C-terminal tagging, whereas the sfGFP-mCherry timer – for N-terminal tagging. For internal tagging, both timers should be tested to first identify the degradation initiation site based on the size of processed tFT fragments.

(ii) Generally, a tFT in which both FPs are efficiently degraded by the proteasome is preferable, assuming its time range is suitable for the intended analysis. However, tFTs with incomplete proteasomal degradation can be advantageous in some situations. For instance, accumulation of processed tFT fragments should facilitate detection of extremely unstable proteins tagged C-terminally with mCherry-sfGFP.

(iii) Characterization of a new tFT should involve testing both arrangements of FPs as reporters of protein age (e.g. Pma1 assay) and protein degradation (e.g. Ubi-X-tFT assay). This should provide qualitative estimates of FP maturation rates, efficiency of proteasomal degradation and time range for the tFT.

To follow protein dynamics, fast-maturing FP tags are needed to detect proteins as early as possible after synthesis. Our analysis indicates that mNeonGreen (Lam *et al.*, 2012) is a good alternative to sfGFP: it is similarly fast-maturing but significantly less resistant to proteasomal degradation in yeast than sfGFP (Figures 1 and 2). The molecular brightness of mNeonGreen is similar to sfGFP when using excitation/emission wavelengths optimal for sfGFP and ~5 times higher with wavelengths optimal for mNeonGreen (Figure S1). The only limitation is that filter sets matching the excitation/emission peaks of

mNeonGreen or lasers around its 506 nm excitation peak are not commonly used in fluorescence microscopy. The cp8 circular permutation of sfGFP is another alternative. When used as a C-terminal tag, sfGFP(cp8) is completely degraded by the proteasome and its maturation kinetics and brightness are similar to sfGFP (Figure 4).

In conclusion, our study provides a detailed characterization of tFTs as reporters of protein age and degradation. This should facilitate their application in different areas of cellular and organismal research. Our work also emphasizes the notion that fluorescent proteins are not neutral tags. Careful characterization of their properties is required for correct interpretation of protein dynamics measurements across spatial and temporal dimensions.

Materials and Methods

Yeast methods and plasmids

Yeast genome manipulations (gene deletions and tagging) were performed using conventional PCR targeting, as described (Janke *et al.*, 2004). Yeast strains and plasmids used in this study are listed in Supplemental Tables 1 and 2, respectively. Yeast codon-optimized sequences of all fluorescent proteins were obtained using full gene synthesis. All Ubi-X-tFT constructs are based on previously described Ubi-X-β-galactosidase fusions, where X is followed by a 40-residue sequence that starts with histidine (Bachmair *et al.*, 1986). The sequence of the ubiquitin-independent ODC23 degron (MSCAQESITSLYKKAGSENLYFQ) was obtained from plasmid pCT334 (Renicke *et al.*, 2013). The Don1 coding sequence was amplified from genomic DNA of strain ESM356-1 (Supplemental Table 1). Standard site-directed mutagenesis was used to introduce point mutations into sfGFP or Clover and change the linker between mCherry and sfGFP. Circular permutations of sfGFP were amplified from a plasmid carrying two copies of sfGFP fused with a short linker (GSGAG). The N-termini of circular permutations 3, 7, 8, 9, 12 and 13 are the amino acids at position 51, 129, 140, 145, 189 and 189 of sfGFP, respectively. All plasmid sequences are available upon request.

tFT maturation and turnover

Fluorescence intensity curves depicting maturation of a pool of mCherry-sfGFP molecules initialized in the non-mature state in the absence of protein production and degradation (Figure 1A) were calculated using a two-step maturation model for mCherry (maturation half-times of 16.91 and 30.3 min) and one-step maturation model for sfGFP (maturation half-time of 5.63 min), as described (Khmelinskii *et al.*, 2012). To examine the influence of greenFP on tFT maturation (Figure 1B), the maturation half-time of greenFP was varied between 5 and 45 min in 5 min steps. All curves were normalized to the point of complete maturation.

To examine the influence of greenFP maturation on the relationship between protein half-life and mCherry/greenFP intensity ratio in steady state (Figure 2A), mCherry/greenFP intensity ratios were calculated according to equation E33 (Supplemental Theory), using $z = 0$, mCherry maturation half-times of 16.91 and 30.3 min, greenFP maturation half-time between 5 and 45 min varied in 5 min steps and a population doubling time of 90 min.

To examine the influence of incomplete tFT degradation on the relationship between protein half-life and mCherry/greenFP intensity ratio in steady state (Figure 5, A and B), mCherry/greenFP intensity ratios were calculated for mCherry-sfGFP and sfGFP-mCherry timers according to equations E33 and E34 , respectively (Supplemental Theory), using mCherry maturation half-times of 16.91 and 30.3 min for both full-length fusion and processed form, sfGFP maturation half-time of 5.63 min for both full-length fusion and processed form, degradation rate constant of processed tFT $k_2 = 0$, a population doubling time of 90 min and varying the probability of incomplete tFT degradation z between 0 and 1 in steps of 0.1.

Fluorescence microscopy

Strains were grown at 30°C in low fluorescence medium (synthetic complete medium prepared with yeast nitrogen base lacking folic acid and riboflavin (CYN6501, ForMedium)) to 0.4-1.2x10^7 cells ml^{-1} and attached to glass-bottom 96-well plates (MGB096-1-2-LG-L, Matrical) using Concanavalin A (C7275, Sigma) as described (Khmelinskii and Knop, 2014). Images from the middle of the cell were acquired on a DeltaVision Elite system (Applied Precision), consisting of an inverted epifluorescence microscope (IX71; Olympus) equipped with an LED light engine (SpectraX, Lumencor), 475/28 and 575/25 excitation, and 525/50 and 624/40 emission filters (Semrock), a dual-band beam splitter 89021 (Chroma Technology), a 100x NA 1.4

UPlanSApo oil immersion objective (Olympus), an sCMOS camera (pco.edge 4.2, PCO) and a motorized stage contained in a temperature-controlled chamber. Image correction and quantification were performed using ImageJ (Schneider *et al.*, 2012). Dark signal and flat field corrections were applied to all images as described (Khmelinskii and Knop, 2014). Outlines of mother and bud compartments were manually defined in the sfGFP channel using a 5 pixel wide segmented line with a spline fit and applied to the mCherry channel. Fluorescence measurements at the plasma membrane were corrected for background using autofluorescence of the growth medium measured in close proximity to each individual cell.

Flow cytometry

Strains were grown at 30°C in synthetic medium lacking leucine (to select for plasmids) to a density of 0.4-1.2x10^7 cells ml^{-1}. Single cell fluorescence intensities, forward and side scatter were measured for at least 6000 cells per sample on a BD FACSCanto RUO Special Order System (BD Biosciences) equipped with 488 nm and 561 nm lasers, 505 nm and 600 nm long pass filters, 530/30 nm and 610/20 nm band pass filters. Multi-spectral beads (3.0–3.4 µm Sphero Rainbow Calibration Particles (6 peaks), #556286, BD Biosciences) were used to control for fluctuations in excitation laser power. Data analysis was performed with Flowing Software 2 (www.flowingsoftware.com): measurements were gated for cells, followed by gating for cells with fluorescence above background to exclude cells that lost the expression plasmids. Sample measurements were corrected for background using autofluorescence levels of a control strain carrying an empty plasmid. mCherry/sfGFP intensity ratios were calculated for each individual cell.

Colony fluorescence measurements

Strains were grown to saturation at 30°C in synthetic medium lacking leucine and pinned onto agar plates with synthetic medium lacking leucine in 384-colony format, with 4 technical replicates for each strain. For pinning a RoToR pinning robot (Singer Instruments) was used. Fluorescence intensities of colonies were typically measured after 24 h of growth at 30°C using an Infinite M1000 Pro plate reader (Tecan). Measurements in mCherry (587/10 nm excitation, 610/10 nm emission, optimal detector gain) and sfGFP (488/10 nm excitation, 510/10 nm emission, optimal detector gain) channels were performed from the top at 400 Hz frequency of the flash lamp, with 20 flashes averaged for each measurement. For relative measurements of molecular brightness of different greenFPs (Figure S1B), fluorescence intensities were additionally measured in a third channel (505/5 nm excitation, 516/5 nm emission, optimal detector gain). Measurements of control colonies without fluorescent protein expression were used to correct all measurements for background.

To acquire excitation spectra (Figure S1C), exponentially growing cultures of strains yMaM26 and yMaM32 (Supplemental Table 1) were transferred to glass-bottom 96-well plates (MGB096-1-2-LG-L, Matrical) and allowed to settle down. Fluorescence emission at 510/5 nm was measured from the bottom with excitation wavelengths between 350 and 600 nm, in 2 nm steps, at 400 Hz frequency of the flash lamp, with 1 flash per step.

Immunoblotting and time-course experiments

Strains were typically grown at 30°C in synthetic medium lacking leucine to 10^7 cells ml^{-1}. One-milliliter samples were mixed with 150 µl of 1.85 M NaOH and 10 µl β-mercaptoethanol, and flash frozen in liquid nitrogen. Whole cell extracts were prepared as previously described (Knop *et al.*, 1999), separated by SDS-PAGE (NuPAGE Novex 4-12% Bis-Tris protein gels (Life Technologies)) followed by blotting and probed with mouse anti-HA (12CA5), rabbit anti-GFP (ab6556, abcam), rabbit anti-YFP (Miller *et al.*, 2015), mouse anti-Pgk1 (22C5D8, Molecular Probes) and rabbit anti-Zwf1 (Miller *et al.*, 2015) antibodies. Secondary goat anti-mouse (IgG (H+L)-HRP, Dianova) and goat anti-rabbit (IgG (H+L)-HRP, Dianova) antibodies were used for detection on a LAS-4000 system (Fuji).

For cycloheximide chases, strains were grown at 30°C in synthetic complete medium to ~0.8x10^7 cells ml^{-1} before addition of cycloheximide to 100 µg/ml final concentration. One-milliliter samples taken at each time point were immediately mixed with 150 µl of 1.85 M NaOH and 10 µl β-mercaptoethanol, flash frozen in liquid nitrogen and processed for immunoblotting as detailed above.

For the proteasome inhibition experiment (Figure S2C), strains yMaM67 and yMaM957 (Supplemental Table 1) were grown at 30°C to ~0.8x10^7 cells ml^{-1} in synthetic medium lacking leucine and with raffinose (2% w/v) as carbon source. Expression of Ubi-R-mCherry-sfGFP was induced by addition of galactose (2% w/v) alongside inhibition of proteasome activity by addition of MG132 (40 mM stock in DMSO) to 80 µg/ml

final concentration or DMSO as control. Whole cell extracts of samples collected before and after induction were prepared and analyzed by SDS-PAGE followed by immunoblotting, as detailed above.

Supplemental Materials

Supplemental Materials contain Supplemental Theory, Supplemental Figures S1-S3 and Supplemental Tables 1 and 2.

Acknowledgements

We thank Christof Taxis for reagents, Marius Lemberg and Marc Zimmer for comments on the manuscript. This work was supported by the Deutsche Forschungsgemeinschaft (DFG) through the Sonderforschungsbereich 1036 (SFB1036) (M.K., A.M. and B.B.) and the Hartmut Hoffmann-Berling International Graduate School of Molecular and Cellular Biology (HBIGS) (C.H.).

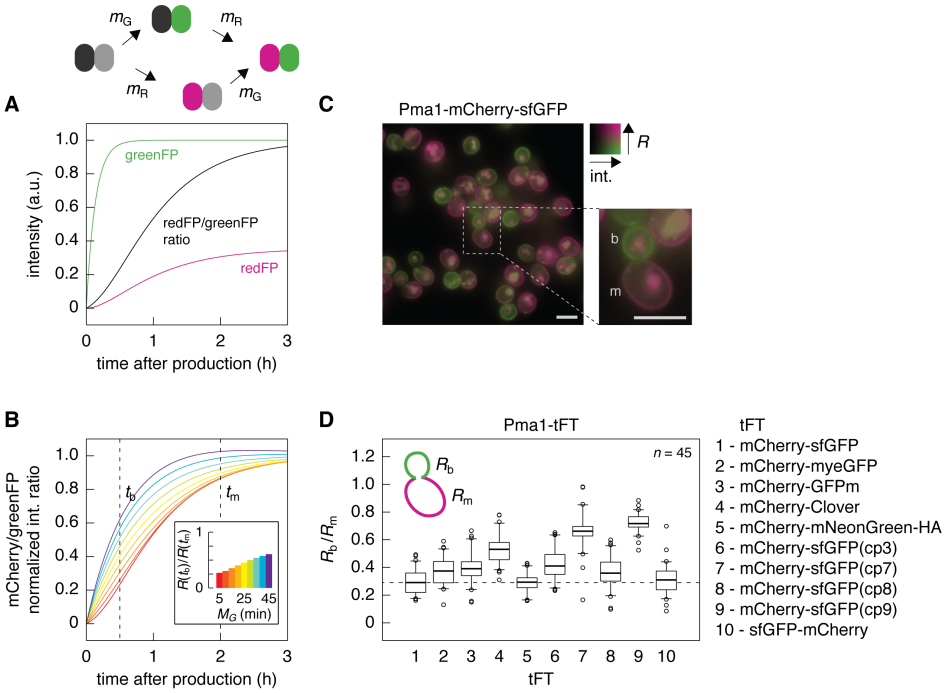

Figure 1. Analysis of protein age with different tFTs.

A – Behavior of a tFT composed of a slower-maturing redFP (black – magenta, maturation rate constant m_R) and a faster-maturing greenFP (grey – green, maturation rate constant m_G). Fluorescence intensity curves were calculated using published maturation parameters for mCherry (redFP) and sfGFP (greenFP) (Khmelinskii *et al.*, 2012) for a population of tFT molecules initialized in the non-mature state in the absence of protein production and degradation. Intensity curves are normalized to the brightness of sfGFP, ratio curve is normalized to the point of complete maturation.

B – tFTs composed of mCherry and greenFPs with different maturation kinetics. mCherry/greenFP intensity ratio curves were calculated as in A using published maturation parameters for mCherry (Khmelinskii *et al.*, 2012) and maturation half-time M_G between 5 and 45 min for greenFP. Note that the maturation half-time M_G is related to the maturation rate constant m_G as $M_G = \ln(2)/m_G$. Each curve is normalized to the point of complete maturation. Inset shows the comparison of mCherry/greenFP intensity ratios (R) for each tFT at two time points: $t_b = 30$ min (approximate age of a bud) and $t_m = 2$ h (approximate age of a young mother cell).

C – Representative intensity-weighted ratiometric image of cells expressing Pma1-mCherry-sfGFP, color-coded according to sfGFP intensity (int.) and mCherry/sfGFP intensity ratio (R). A dividing cell with labeled mother (m) and bud (b) compartments is shown. Scale bars are 5 μm.

D – mCherry/greenFP intensity ratios (R) of Pma1 tagged with the indicated tFTs were measured at the plasma membrane in pairs of mother (R_m) and bud (R_b) cells ($n = 45$ pairs for each tFT). Center lines mark the medians, box limits indicate the 25th and 75th percentiles, whiskers extend to 5th and 95th percentiles. The difference between R_m and R_b is significant for all tFTs ($p < 10^{-19}$ in a paired t-test). The mCherry-mNeonGreen timer carried a C-terminal hemagglutinin epitope (HA) tag to facilitate detection by immunoblotting.

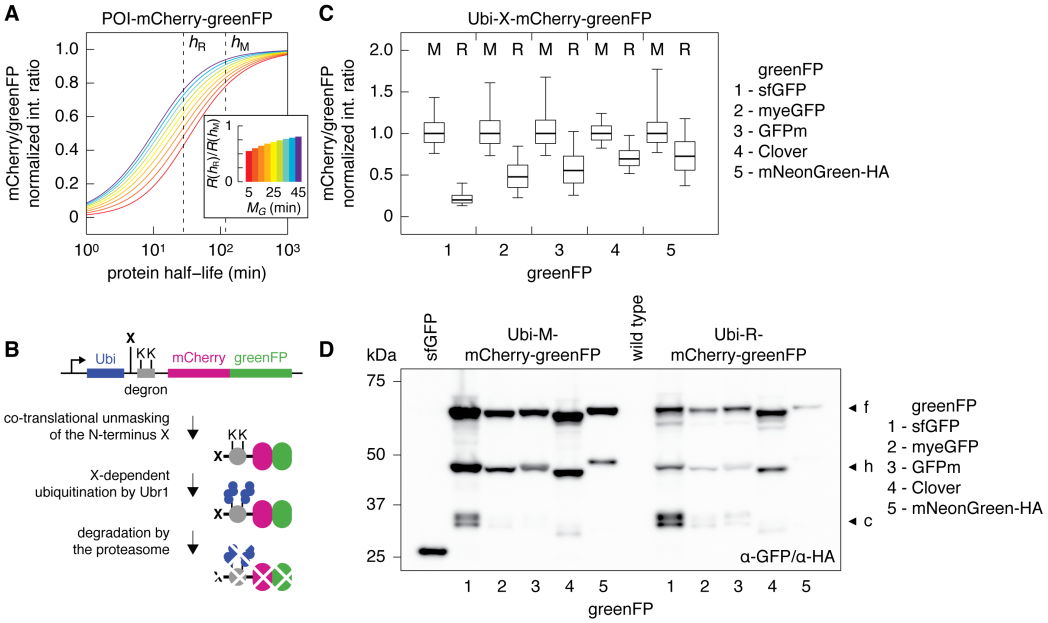

Figure 2. Analysis of protein degradation kinetics with different tFTs.

A – Relationship between half-life of a tFT protein fusion and mCherry/greenFP intensity ratio in steady state. mCherry/greenFP intensity ratios were calculated as a function of protein degradation kinetics for a population doubling time of 90 min using published maturation parameters for mCherry (Khmelinskii *et al.*, 2012) and maturation half-time M_G between 5 and 45 min for greenFP. Each curve is normalized to the mCherry/sfGFP intensity ratio of a non-degradable tFT fusion. Note that protein half-life T is related to degradation rate constant k as $T = \ln(2)/k$. Similarly, maturation half-time M_{G} is related to maturation rate constant m_{G} as $M_{\mathrm{G}} = \ln(2)/m_{\mathrm{G}}$. Inset shows the comparison of mCherry/greenFP intensity ratios (R) obtained with each tFT for two protein half-lives: $h_{\mathrm{R}} = 28$ min (half-life of R-mCherry-sfGFP) and $h_{\mathrm{M}} = 119$ min (half-life of M-mCherry-sfGFP) (Figure S2B).

B – Cartoon of Ubi-X-mCherry-greenFP constructs. Degradation rate of X-mCherry-greenFP fusions depends on the residue X, such that X = T (slow) < M < I < Y < F < R (fast).

C – Fluorescence measurements with flow cytometry of strains expressing the indicated Ubi-X-mCherry-greenFP fusions. The residue X in each fusion is specified in the plot. Fusions with mNeonGreen carried a C-terminal HA tag to facilitate detection by immunoblotting. For each tFT, the mCherry/greenFP intensity ratios of individual cells were normalized to the median mCherry/greenFP intensity ratio of the corresponding Ubi-M-mCherry-greenFP fusion. Center lines mark the medians, box limits indicate the 25th and 75th percentiles, whiskers extend to 5th and 95th percentiles.

D – Immunoblot of strains expressing the indicated constructs. Whole cell extracts were separated by SDS-PAGE and probed with a mixture of antibodies against GFP and the HA tag. Three major forms observed for each Ubi-X-mCherry-greenFP fusion are indicated: a full-length X-mCherry-greenFP form (f), a shorter mCherry$^{\Delta N}$-greenFP product resulting from mCherry autohydrolysis during cell extract preparation (h) (Baird *et al.*, 2000) and fast-migrating processed tFT fragments (c).

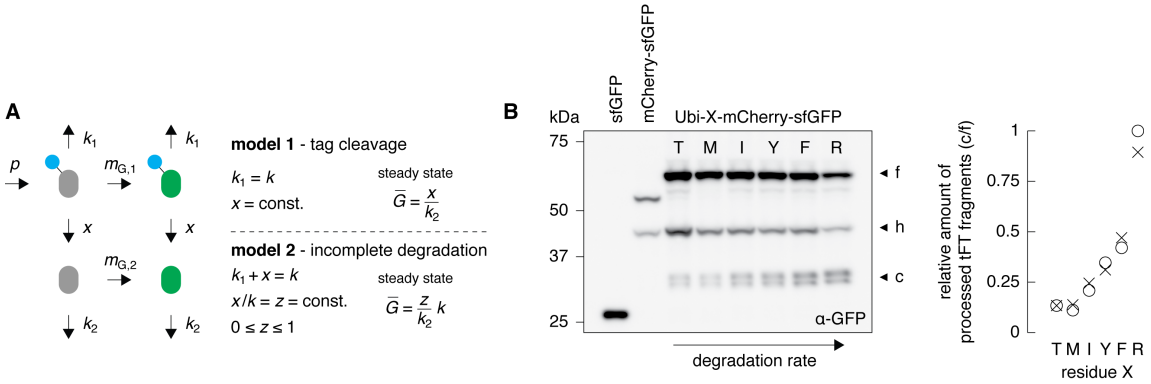

Figure 3. Incomplete degradation of tFT fusions leads to accumulation of processed tFT fragments.

A – Turnover of a greenFP protein fusion with accumulation of processed greenFP. We assume that a greenFP protein fusion (protein of interest, represented by a blue circle, tagged with a greenFP) is produced at a constant rate p as a non-fluorescent protein and matures to a fluorescent protein in a single step with maturation rate constant $m_{G,1}$. In model 1, greenFP protein fusions are degraded with rate constant k and greenFP can be cleaved off from both non-mature and mature protein fusions with rate constant x. In model 2, degradation of greenFP protein fusions with rate constant k proceeds to completion with probability $1 - z$, such that greenFP fusions are effectively degraded with rate constant $k_1 = (1 - z)k$ and processed greenFP is produced with rate constant $x = kz$. Processed non-fluorescent greenFP matures in a single step with maturation rate constant $m_{G,2}$ and is degraded with rate constant k_2 in both models. In steady state, the fraction of processed greenFP ($\bar{G}$, defined as the ratio between the total number of processed greenFP molecules and the total number of greenFP protein fusion molecules) is independent of k in model 1. However, $\bar{G}$ is proportional to k in model 2. Further details are provided as Supplemental Theory.

B – Immunoblot of strains expressing the indicated constructs. The residue X in each Ubi-X-mCherry-sfGFP fusion is specified in the immunoblot. Three major forms observed for each Ubi-X-mCherry-sfGFP fusion are indicated as in Figure 2D. Note that in agreement with their degradation-dependent origin, processed tFT fragments were not detected in the strain expressing the stable mCherry-sfGFP fusion. The c/f ratio between the intensities of the (c) and (f) bands measured for each strain in two independent immunoblots, normalized to the maximum c/f ratio, is shown in the right panel.

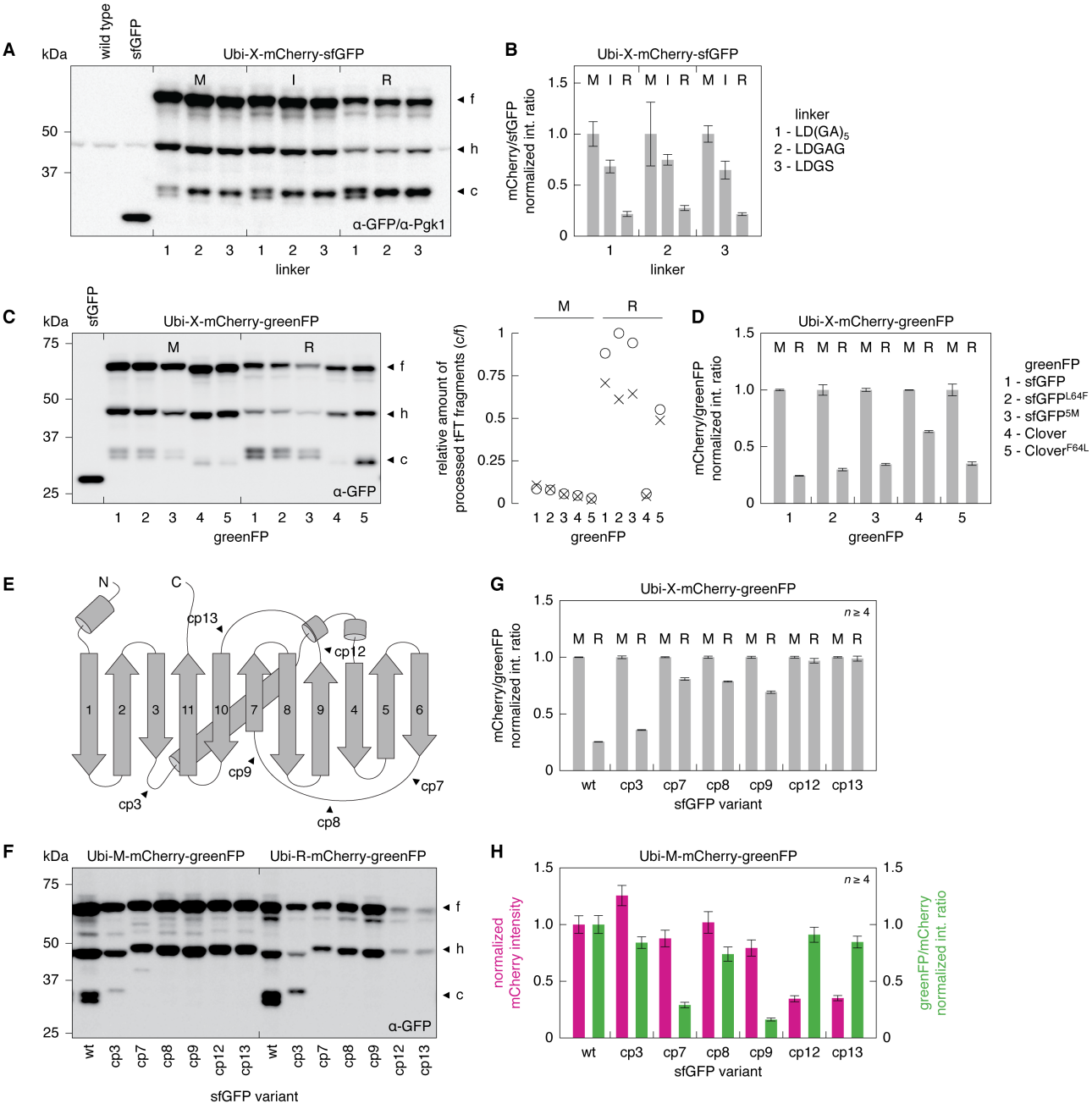

Figure 4. Stable greenFP fold prevents complete degradation of tFT fusions.

A – Immunoblot of strains expressing Ubi-X-mCherry-sfGFP constructs with the indicated linkers between mCherry and sfGFP. The residue X in each Ubi-X-mCherry-sfGFP fusion is specified in the immunoblot. Whole cell extracts were separated by SDS-PAGE and probed with antibodies against GFP and Pgk1 as loading control. Three major forms observed for each Ubi-X-mCherry-sfGFP fusion are indicated as in Figure 2D. Note that the bands corresponding to Pgk1 and the (h) form overlap.

B – mCherry/sfGFP intensity ratios determined from whole colony fluorescence measurements of strains expressing Ubi-X-mCherry-sfGFP constructs in A. For each linker, mCherry/sfGFP intensity ratios (mean ± s.d., $n \geq 12$ per construct) were normalized to the corresponding Ubi-M-mCherry-sfGFP fusion.

C – Immunoblot of strains expressing Ubi-X-mCherry-greenFP constructs with the indicated greenFPs. The residue X in each Ubi-X-mCherry-greenFP fusion is specified in the immunoblot. Three major forms observed for each fusion are indicated as in Figure 2D. The c/f ratio between the intensities of the (c) and (f) bands measured for each strain in two independent immunoblots, normalized to the maximum c/f ratio, is shown in the right panel.

D – mCherry/sfGFP intensity ratios determined from whole colony fluorescence measurements of strains expressing Ubi-X-mCherry-greenFP constructs in C. For each greenFP, mCherry/greenFP intensity ratios (mean ± s.d., $n \geq 4$ per construct) were normalized to the corresponding Ubi-M-mCherry-greenFP fusion.

E – Schematic representation of sfGFP. Start sites of six circular permutations (cp) are indicated, numbered according to (Pédelacq *et al.*, 2006).

F – Immunoblot of strains expressing Ubi-X-mCherry-greenFP constructs with different circular permutations of sfGFP as greenFP. Three major forms observed for each fusion are indicated as in Figure 2D.

G, H – Whole colony fluorescence measurements of strains expressing Ubi-X-mCherry-greenFP constructs in F. G – The residue X in each fusion is specified in the plot. For each sfGFP variant, mCherry/greenFP intensity ratios (mean ± s.d., $n \geq 4$ per construct) were normalized to the corresponding Ubi-M-mCherry-greenFP fusion. H – mCherry fluorescence intensities (measure of expression levels) and greenFP/mCherry intensity ratios (measure of greenFP molecular brightness) (mean ± s.d., $n \geq 4$ per construct) were normalized to Ubi-M-mCherry-sfGFP.

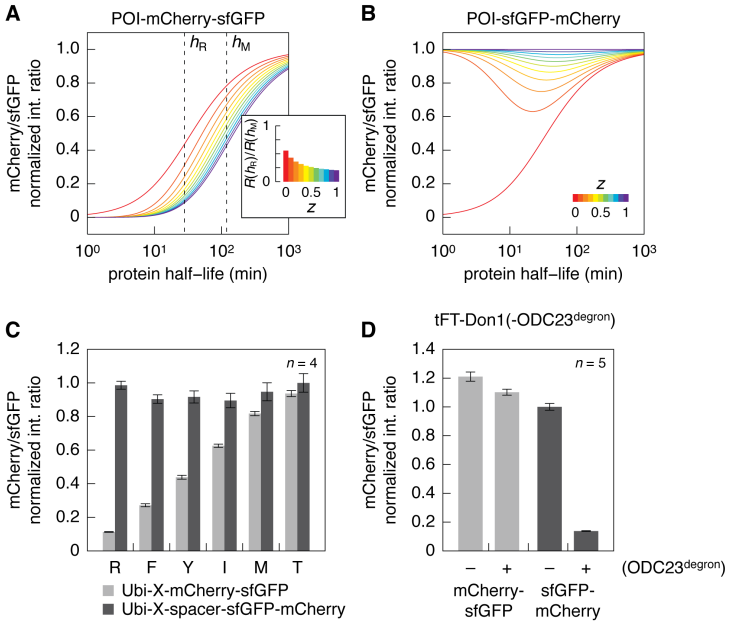

Figure 5. Proteasome-dependent processing constrains the design of tFTs.

A, B – Relationship between half-life of a protein of interest (POI) tagged at the C-terminus with a tFT and mCherry/sfGFP intensity ratio in steady state. mCherry/sfGFP intensity ratios were calculated as a function of protein degradation kinetics for a population doubling time of 90 min using published maturation parameters for mCherry and sfGFP (Khmelinskii *et al.*, 2012) and probability z of incomplete degradation of sfGFP between 0 and 1. Incomplete degradation produces free sfGFP in A or free sfGFP-mCherry in B. Each curve is normalized to the mCherry/sfGFP intensity ratio of a non-degradable tFT fusion. Further details are provided as Supplemental Theory. Inset shows the comparison of mCherry/sfGFP intensity ratios (R) obtained with each z for two protein half-lives: $h_{\mathrm{R}} = 28$ min (half-life of R-mCherry-sfGFP) and $h_{\mathrm{M}} = 119$ min (half-life of M-mCherry-sfGFP) (Figure S2B).

C – Fluorescence measurements with flow cytometry of strains expressing the indicated Ubi-X-tFT fusions. The residue X in each fusion is specified in the plot. mCherry/sfGFP intensity ratios (mean ± s.d., $n = 4$ per construct) were normalized to Ubi-T-spacer-sfGFP-mCherry.

D – Whole colony fluorescence measurements of strains expressing tFT-Don1 fusions with and without an ODC23 degron at the C-terminus. The tFT in each fusion is specified in the plot. mCherry/sfGFP intensity ratios (mean ± s.d., $n = 5$ per construct) were normalized to sfGFP-mCherry-Don1.

References

Aviram, S., and Kornitzer, D. (2010). The ubiquitin ligase Hul5 promotes proteasomal processivity. Mol. Cell. Biol. *30*, 985–994.

Bachmair, A., Finley, D., and Varshavsky, A. (1986). In vivo half-life of a protein is a function of its amino-terminal residue. Science *234*, 179–186.

Baird, G. S., Zacharias, D. A., and Tsien, R. Y. (1999). Circular permutation and receptor insertion within green fluorescent proteins. Proc. Natl. Acad. Sci. U.S.a. *96*, 11241–11246.

Baird, G. S., Zacharias, D. A., and Tsien, R. Y. (2000). Biochemistry, mutagenesis, and oligomerization of DsRed, a red fluorescent protein from coral. Proc. Natl. Acad. Sci. U.S.a. *97*, 11984–11989.

Chu, B. W., Kovary, K. M., Guillaume, J., Chen, L.-C., Teruel, M. N., and Wandless, T. J. (2013). The E3 ubiquitin ligase UBE3C enhances proteasome processivity by ubiquitinating partially proteolyzed substrates. Journal of Biological Chemistry *288*, 34575–34587.

Cormack, B. P., Valdivia, R. H., and Falkow, S. (1996). FACS-optimized mutants of the green fluorescent protein (GFP). Gene *173*, 33–38.

Daskalogianni, C., Apcher, S., Candeias, M. M., Naski, N., Calvo, F., and Fåhraeus, R. (2008). Gly-Ala repeats induce position- and substrate-specific regulation of 26 S proteasome-dependent partial processing. J. Biol. Chem. *283*, 30090–30100.

Dean, K. M., and Palmer, A. E. (2014). Advances in fluorescence labeling strategies for dynamic cellular imaging. Nat Chem Biol *10*, 512–523.

Dona, E. *et al.* (2013). Directional tissue migration through a self-generated chemokine gradient. Nature *503*, 285–289.

Fishbain, S., Inobe, T., Israeli, E., Chavali, S., Yu, H., Kago, G., Babu, M. M., and Matouschek, A. (2015). Sequence composition of disordered regions fine-tunes protein half-life. Nat. Struct. Mol. Biol. *22*, 214–221.

Hoyt, M. A., Zich, J., Takeuchi, J., Zhang, M., Govaerts, C., and Coffino, P. (2006). Glycine-alanine repeats impair proper substrate unfolding by the proteasome. Embo J. *25*, 1720–1729.

Huang, J.-R., Craggs, T. D., Christodoulou, J., and Jackson, S. E. (2007). Stable intermediate states and high energy barriers in the unfolding of GFP. J. Mol. Biol. *370*, 356–371.

Iizuka, R., Yamagishi-Shirasaki, M., and Funatsu, T. (2011). Kinetic study of de novo chromophore maturation of fluorescent proteins. Anal. Biochem. *414*, 173–178.

Janke, C. *et al.* (2004). A versatile toolbox for PCR-based tagging of yeast genes: new fluorescent proteins, more markers and promoter substitution cassettes. Yeast *21*, 947–962.

Khmelinskii, A. *et al.* (2012). Tandem fluorescent protein timers for in vivo analysis of protein dynamics. Nat. Biotechnol. *30*, 708–714.

Khmelinskii, A., and Knop, M. (2014). Analysis of protein dynamics with tandem fluorescent protein timers. Methods Mol. Biol. *1174*, 195–210.

Klionsky, D. J. *et al.* (2008). Guidelines for the use and interpretation of assays for monitoring autophagy in higher eukaryotes. Autophagy *4*, 151–175.

Knop, M., Siegers, K., Pereira, G., Zachariae, W., Winsor, B., Nasmyth, K., and Schiebel, E. (1999). Epitope tagging of yeast genes using a PCR-based strategy: more tags and improved practical routines. Yeast *15*, 963–972.

Kraut, D. A., Israeli, E., Schrader, E. K., Patil, A., Nakai, K., Nanavati, D., Inobe, T., and Matouschek, A. (2012). Sequence- and species-dependence of proteasomal processivity. ACS Chem. Biol. *7*, 1444–1453.

Lam, A. J. *et al.* (2012). Improving FRET dynamic range with bright green and red fluorescent proteins. Nature Methods *9*, 1005–1012.

Malínská, K., Malínský, J., Opekarová, M., and Tanner, W. (2003). Visualization of protein compartmentation within the plasma membrane of living yeast cells. Mol. Biol. Cell *14*, 4427–4436.

Martínez-Noël, G., Galligan, J. T., Sowa, M. E., Arndt, V., Overton, T. M., Harper, J. W., and Howley, P. M. (2012). Identification and proteomic analysis of distinct UBE3A/E6AP protein complexes. Mol. Cell. Biol. *32*, 3095–3106.

Miller, S. B. M. *et al.* (2015). Compartment-specific aggregases direct distinct nuclear and cytoplasmic aggregate deposition. Embo J. *34*, 778–797.

Nager, A. R., Baker, T. A., and Sauer, R. T. (2011). Stepwise unfolding of a β barrel protein by the AAA+ ClpXP protease. J. Mol. Biol. *413*, 4–16.

Pédelacq, J.-D., Cabantous, S., Tran, T., Terwilliger, T. C., and Waldo, G. S. (2006). Engineering and characterization of a superfolder green fluorescent protein. Nat. Biotechnol. *24*, 79–88.

Prakash, S., Tian, L., Ratliff, K. S., Lehotzky, R. E., and Matouschek, A. (2004). An unstructured initiation site is required for efficient proteasome-mediated degradation. Nat. Struct. Mol. Biol. *11*, 830–837.

Renicke, C., Schuster, D., Usherenko, S., Essen, L.-O., and Taxis, C. (2013). A LOV2 domain-based optogenetic tool to control protein degradation and cellular function. Chem. Biol. *20*, 619–626.

Schneider, C. A., Rasband, W. S., and Eliceiri, K. W. (2012). NIH Image to ImageJ: 25 years of image analysis. Nature Methods *9*, 671–675.

Schrader, E. K., Harstad, K. G., and Matouschek, A. (2009). Targeting proteins for degradation. Nat Chem Biol *5*, 815–822.

Shaner, N. C. *et al.* (2013). A bright monomeric green fluorescent protein derived from Branchiostoma lanceolatum. Nature Methods *10*, 407–409.

Shaner, N. C., Campbell, R. E., Steinbach, P. A., Giepmans, B. N. G., Palmer, A. E., and Tsien, R. Y. (2004). Improved monomeric red, orange and yellow fluorescent proteins derived from Discosoma sp. red fluorescent protein. Nat. Biotechnol. *22*, 1567–1572.

Shaner, N. C., Steinbach, P. A., and Tsien, R. Y. (2005). A guide to choosing fluorescent proteins. Nature Methods *2*, 905–909.

Shintani, T., and Klionsky, D. J. (2004). Cargo proteins facilitate the formation of transport vesicles in the cytoplasm to vacuole targeting pathway. J. Biol. Chem. *279*, 29889–29894.

Takizawa, P. A., DeRisi, J. L., Wilhelm, J. E., and Vale, R. D. (2000). Plasma membrane compartmentalization in yeast by messenger RNA transport and a septin diffusion barrier. Science *290*, 341–344.

Thayer, N. H., Leverich, C. K., Fitzgibbon, M. P., Nelson, Z. W., Henderson, K. A., Gafken, P. R., Hsu, J. J., and Gottschling, D. E. (2014). Identification of long-lived proteins retained in cells undergoing repeated asymmetric divisions. Proc Natl Acad Sci USA *111*, 14019–14026.

Topell, S., Hennecke, J., and Glockshuber, R. (1999). Circularly permuted variants of the green fluorescent protein. FEBS Lett. *457*, 283–289.

Tsien, R. Y. (1998). The green fluorescent protein. Annu. Rev. Biochem. *67*, 509–544.

Varshavsky, A. (2011). The N-end rule pathway and regulation by proteolysis. Protein Sci. *20*, 1298–1345.

Yoo, T. H., Link, A. J., and Tirrell, D. A. (2007). Evolution of a fluorinated green fluorescent protein. Proc. Natl. Acad. Sci. U.S.a. *104*, 13887–13890.

Zacharias, D. A., Violin, J. D., Newton, A. C., and Tsien, R. Y. (2002). Partitioning of lipid-modified monomeric GFPs into membrane microdomains of live cells. Science *296*, 913–916.

Zhang, M., and Coffino, P. (2004). Repeat sequence of Epstein-Barr virus-encoded nuclear antigen 1 protein interrupts proteasome substrate processing. J. Biol. Chem. *279*, 8635–8641.

Zimmer, M. H., Li, B., Shahid, R. S., Peshkepija, P., and Zimmer, M. (2014). Structural consequences of chromophore formation and exploration of conserved lid residues amongst naturally occurring fluorescent proteins. Chem Phys *429*, 5–11.